Oscillation-Free Adaptive Simulation of Compressible Two-Fluid Flows with Different Types of Equation of State

H.W. Zheng, C. Shu, Y.T. Chew, and N. Qin

Abstract In many situations, the equations of state (EOS) found in the literature have only a limited range of validity. Besides, different types of EOS are required for different fluids of compressible multi-fluid flows. These inspire us to investigate compressible multi-fluid flows with different types of equation of state (EOS). In this paper, the oscillation-free adaptive method for compressible two-fluid flows with different types of equation of state (EOS) is proposed. By using a general form of EOS instead of solving the non-linear equation, the pressure of the mixture can be analytically calculated for compressible multi-fluid flows with different types of EOS. It is proved that it preserves the oscillation-free property across the interface. To capture the interface as fine as sharp interface, the quadrilateral-cell based adaptive mesh is employed. In this adaptive method, the cells with different levels are stored in different lists. This avoids the recursive calculation of solution of mother (non-leaf) cells. Moreover, the edges are separated stored into two lists for leaf edges and non-leaf edges respectively. Hence, there is no need to handle the handing nodes and no special treatment at the interface between the finer cell and the coarse cell. Thus, high efficiency is obtained due to these features. To examine its performance in solving the various compressible two-fluid flow problems with two different types of EOS, the interface translation and bubble shock interaction case with different types of EOS are employed. The results show that it can adaptively and accurately solve these problems and especially preserve the oscillation-free property of pressure and velocity across the material interface.

H.W. Zheng (✉)
LHD, Institute of Mechanics, Chinese Academy of Sciences, Beijing 100190, China
e-mail: H.Zheng@sheffield.ac.uk

N. Qin
Department of Mechanical Engineering, University of Sheffield, Mappin Street, Sheffield S1 3JD, UK

C. Shu · Y.T. Chew
Department of Mechanical Engineering, National University of Singapore, 10 Kent Ridge Crescent, Singapore 119260, Singapore

F.C.G.A. Nicolleau et al. (eds.), *New Approaches in Modeling Multiphase Flows and Dispersion in Turbulence, Fractal Methods and Synthetic Turbulence*,
ERCOFTAC Series 18, DOI 10.1007/978-94-007-2506-5_7,

1 Introduction

In the past years, many works have been proposed for the modeling of compressible two-fluid flows [1–15]. However, there are still some challenging issues such as the modeling of compressible multi-fluid flows with different types of equation of state (EOS) and the capturing of the interface as fine as sharp interface etc. The more difficult one is to combine these two factors as well as preserve the oscillation-free property.

To tackle the problems with different types of EOS, there are three main methods: front tracking method [1], ghost fluid method [2–4] and the fluid mixture or diffuse interface methods [5–8]. Among them, the third one is the popular one that can be easily implemented and needs not track the interface explicitly. The main issues for this kind of method are the derivation of the variables to capture the interface and the evaluation of the pressure of the mixture where the different fluids co-exist. Shyue [5] uses the material based variables to track the interface in order to preserve the oscillation-free property across the interface. Besides, it uses a general EOS of the van der Waals and the stiffened gas EOS to calculate the mixture pressure. However, it can only be used to model the two-fluid problems with the van der Waals and the stiffened gas EOS. In his another paper [6], the mixture pressure is calculated by the Mie-Gruneisen EOS where the parameters are a simple summation of the correspondent two parameters of the EOS for each fluid. Thus, it may not preserve the oscillation-free property. Besides, it can only be used to model the two-fluid problems with the Mie-Gruneisen EOS (for example, the Cochran-Chan EOS and the Jones-Wilkins-Lee (JWL) EOS). As compared to the Shyue-type model [5, 6], the methods in [7, 8] only use the volume fraction of each fluid as a dependent variable to capture the interface. Obviously, the transport equation does not depend on the types of EOS. In [7], the mixture pressure is expressed as a volume average of the pressure of each fluids. This will cause the oscillation of velocity and pressure across the interface. While, the calculation of the mixture pressure in the five equation model [8] is different from that in [7] although the five equation model can be regarded as a reduced model of seven equation model. For the flows with two different types of EOS, the mixture pressure is obtained by solving the nonlinear algebraic equation with some type of iterative method [8] in order to preserve the oscillation-free properties of the interface. This procedure is time-consuming. Moreover, the numerical algorithm used in [8] is not very robust and there can be some nonphysical overshot or undershot in the velocity or pressure profile.

To capture of the interface as fine as sharp interface, the adaptive mesh technique is frequently employed. Although there are adaptive mesh methods, only several works [3, 4, 9, 10] has been done on the extension and applications to compressible multi-fluid flows. In order to deal with problems with different types of EOS, most of them combines the idea of ghost fluid method. For example, [3, 4] presented the work by combining the ghost fluid method and the Cartesian adaptive meshes. However, it is not easy to be applied to problems with complex geometry due to the use of structured meshes. Besides, as reported by Nourgaliev et al. [3], the coarse-to-fine and fine-to-coarse inter-level transfer operators are very complicated and may

violate the stability of the code. In order to be extended to the applications in the complex geometry, Banks et al. [9] proposed a method by solving the ghost fluid method on the adaptive Cartesian mesh methods with overlapping mesh. However, the mass or momentum may not be conserved in all these adaptive methods since ghost fluid method employs the level set method to track the interface.

In this paper, to tackle these two problems, the combination of the extended five-equation fluid mixture model and the unstructured adaptive technique [10] is employed. Instead of solving the non-linear equation, we extend the work of Allaire et al. [8] by using a general form of EOS. Thus, the pressure of the mixture can be analytically calculated for compressible multi-fluid flows with different types of EOS. Besides, instead of the Roe scheme for the Euler equations and a simple upwind scheme for the interface transport equation employed in [8], the robust and efficient HLLC scheme [10] is extended to solve the five equation model. To obtain a stable second order extension in space, different interpolation variables are adopted, which are different from the variables in [8]. The quadrilateral unstructured adaptive technique proposed by Zheng et al. [10], is incorporated in the computation. In contrast to [3], there are no the coarse-to-fine and fine-to-coarse inter-level transfer operators. Besides, it could be used for applications with complex geometry.

The rest of this paper is organized as follows. In the second section, based on the proposed general form of EOS, the thermodynamic properties such as the pressure of the mixture could be derived. The proof of the oscillation-free of this model is also given in the second section. Then, in the third section, the numerical discretization of the governing equations on unstructured adaptive meshes is presented. The validation cases for compressible multi-fluid problem with different types of EOS are provided in the fourth section. Numerical examples show that the present method can adaptively and accurately solve multi-fluid flow problems with different types of EOS as well as preserve the oscillation-free property of the pressure and velocity profiles across the material interface.

2 Compressible Two-Fluid Flows

In this section, the compressible two-fluid flows that all pure fluid components can be described by a single velocity and a single pressure function are considered. The compressible multi-fluid flows [8] are governed by the conservation laws

$$\partial_t \int_\Omega \begin{pmatrix} z_0\rho_0 \\ z_1\rho_1 \\ \rho\mathbf{u} \\ E \end{pmatrix} dV + \int_{\partial\Omega} \begin{pmatrix} z_0\rho_0\mathbf{u} \\ z_1\rho_1\mathbf{u} \\ \rho\mathbf{u}\otimes\mathbf{u} + P[I] \\ (E+P)\mathbf{u} \end{pmatrix} \cdot \mathbf{n}\, dS = 0, \tag{1}$$

and a transport equation of the volume fraction of fluid,

$$\frac{\partial z}{\partial t} + \mathbf{u}\cdot\nabla z = 0. \tag{2}$$

Here, ρ is the mixture density, $\mathbf{u}$ the flow velocity, E the total energy ($E = \rho e + 0.5\rho\mathbf{u}^2$, $[I]$ the identity tensor, ρ_i and z_i ($z_0 = z$, $z_1 = 1 - z$) the density and the

volume fraction of fluid i respectively. P is the mixture pressure which is a function of the densities and energies of all fluids $P(\rho_0, \rho_1, \rho e, z)$. The mixture density is calculated by a volume averaging of the densities of each fluid,

$$\rho = \sum_i z_i \rho_i. \tag{3}$$

To close the system, the mixture pressure needs to be determined. It is evaluated in an implicit way [8] by assuming that the pressure for each fluid is equal to each other in the mixture and the mixture internal energy is a linear combination of the internal energies of each fluid. That is,

$$p_i(\rho_i, \rho_i e_i) = P, \quad i = 0, 1, \tag{4}$$

and

$$\rho e = \sum_i z_i \rho_i e_i. \tag{5}$$

2.1 Modeling with General Form of Equation of State

Due to the limited range of validity for a certain types of EOS, it is quite common that several types of EOS for different fluids are involved in many practical applications of compressible multi-fluid flows. This inspires us to investigate compressible multi-fluid flows with different types of equation of state (EOS). For these flows, in Allaire et al. [8], some type of iterative method is required to solve the above non-linear algebraic equation (4). This procedure is usually time consuming.

In this section, we propose a general algorithm on modeling the flows with different analytical types of EOS. Although there are different types of EOS, it could be written in a general algebraic form of EOS,

$$p_i(\rho_i e_i, \rho) = \big[\Gamma_i(\rho_i) - 1\big]\rho_i e_i - \Pi_i(\rho_i). \tag{6}$$

Here, Γ_i and Π_i are the functions to be determined according to the type of EOS.

Taken the general van der Waals gas EOS as an example, if we set,

$$\Gamma_i(\rho_i) = \left(\frac{\gamma_i - 1}{1 - b_i \rho_i}\right) + 1, \tag{7}$$

and

$$\Pi_i(\rho_i) = \left[1 - \left(\frac{\gamma_i - 1}{1 - b_i \rho_i}\right)\right] a_i \rho_i^2 + \left(\frac{\gamma_i - 1}{1 - b_i \rho_i} + 1\right) c_i, \tag{8}$$

we have the general van der Waals gas EOS [5, 8],

$$p_i = \left(\frac{\gamma_i - 1}{1 - b_i \rho_i}\right)\left(\rho_i e_i + a_i \rho_i^2 - c_i\right) - \left(a_i \rho_i^2 + c_i\right). \tag{9}$$

Similarly, it is easy to verify that this form of EOS is a general form of most of the EOS, such as the van der Waals gas, the rarefied gas, the stiffened gas, the Tait's, and the Mie-Gruneisen materials EOS and so on.

According to Eq. (5) and the iso-baric assumption (4), the analytic pressure for the mixture is obtained

$$P(\rho_0, \rho_1, \rho e, z) = \left[\Im(\rho_0, \rho_1, z) - 1\right]\rho e - \aleph, \tag{10}$$

with

$$\Im(\rho_0, \rho_1, z) = 1 + 1/\sum_i \left[z_i \xi_i(\rho_i)\right], \tag{11}$$

$$\aleph(\rho_0, \rho_1, z) = \sum_i \left[z_i \xi_i(\rho_i) \Pi_i(\rho_i)\right] / \sum_i \left[z_i \xi_i(\rho_i)\right], \tag{12}$$

$$\xi_i(\rho_i) = 1/\left[\Gamma_i(\rho_i) - 1\right]. \tag{13}$$

2.2 Oscillation-Free Analysis

A physically consistent model should preserve the oscillation-free property if the viscous, heat transfer and surface tension effects are neglected [5–15]. This oscillation free property means that the velocity and pressure should stay continuous across interfaces,

$$\Delta \mathbf{u} = 0, \qquad \Delta P = 0. \tag{14}$$

Thus, in this section, we try to prove the preservation of oscillation-free of the present model. The upwind discretization of Eq. (1) across interfaces reads,

$$\delta \begin{pmatrix} z_0\rho_0 \\ z_1\rho_1 \\ \rho \mathbf{u} \\ E \end{pmatrix} = -\chi \Delta \begin{pmatrix} u_n z_0 \rho_0 \\ u_n z_1 \rho_1 \\ \rho \mathbf{u} u_n + P\mathbf{n} \\ u_n (E + P) \end{pmatrix}, \tag{15}$$

where $\delta(\,)$ denotes the time changes $(\,)^{n+1} - (\,)^n$, $u_n = \mathbf{u} \cdot \mathbf{n}$ is the normal velocity at the directional edge with the normal direction $\mathbf{n}$, χ is the ratio of the time interval to the space, and $\Delta(\,)$ denotes the spatial changes.

Similarly, Eq. (2) can be discretized as,

$$\delta z = -\chi u_n \Delta z. \tag{16}$$

For the interface evolution problem, there is no jump of densities and energies for each fluid across the interface,

$$\Delta \rho_i = 0, \qquad \Delta e_i = 0. \tag{17}$$

By using Eq. (17) and Eq. (14), one can obtain,

$$\delta \begin{pmatrix} z_0\rho_0 \\ z_1\rho_1 \\ \rho \\ \rho\mathbf{u} \\ E \end{pmatrix} = \begin{pmatrix} -\chi u_n \rho_0 \Delta z_0 \\ -\chi u_n \rho_1 \Delta z_1 \\ -\chi u_n \Delta\rho \\ \mathbf{u}\delta\rho \\ -\chi u_n \Delta E \end{pmatrix}. \tag{18}$$

From Eq. (16) and the first two entries of the above equation (18), we have

$$\delta\rho_i = 0. \tag{19}$$

From the fourth entry of Eq. (18),

$$\delta\mathbf{u} = 0. \tag{20}$$

In order to have the oscillation-free property, it requires that

$$\delta P = 0. \tag{21}$$

Besides, from Eqs. (4), (6), (19), and (21), we have

$$\delta e_i = 0. \tag{22}$$

From Eq. (20) and the last entry of Eq. (18), we have

$$\delta(\rho e) = -\chi u_n \Delta(\rho e). \tag{23}$$

According to Eqs. (5), (17), (19), and (22), it is easy to find that the discretization of the internal energy (23) is equivalent to,

$$\delta z_i = -\chi u_n \Delta z_i. \tag{24}$$

It is clear that Eqs. (24) is consistent with Eq. (2). These show that the present model is oscillation-free.

Note that Eq. (23) is not guaranteed to be satisfied if the mixture pressure is evaluated as the way in [7]

$$P(\rho_0, \rho_1, \rho e, z) = \sum_i z_i\, p_i(\rho_i, \rho_i e_i). \tag{25}$$

Thus, the model in [7] which uses Eq. (25) does not preserve of oscillation-free property.

3 Discretization on Quadrilateral-Cell Based Adaptive Mesh

In order to capture the interface accurately, the unstructured quadrilateral-cell based adaptive technique by Zheng et al. [10] is incorporated in the computation. Thus, the numerical discretization of Eq. (1) and Eq. (2) should be performed on this quadrilateral-cell based adaptive mesh.

In this method, in order to avoid the recursive calculation, the cells are separately stored in different lists according to their levels (Fig. 1(a)). Thus, the solution can

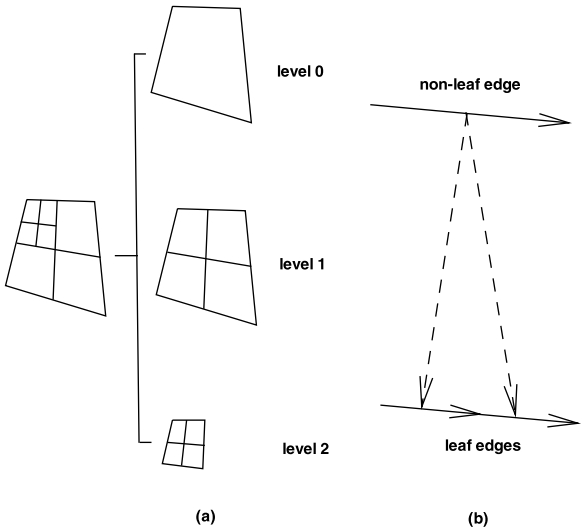

Fig. 1 The cells and edges in adaptive mesh generation [10]

be obtained in a level by level manner so that the cells of high level are calculated after the cells of low level. The set of Eq. (1) and Eq. (2) is only discretized at each leaf cell c by the two stage Runge-Kutta schemes [10],

$$U_c^{(*)} = U_c^n - \alpha \,\mathrm{Res}_c\big(U_c^n\big), \tag{26}$$

and

$$U_c^{n+1} = 0.5\big[U_c^n + U_c^{(*)} - \alpha \,\mathrm{Res}_c\big(U_c^{(*)}\big)\big], \tag{27}$$

where U is the state vector $(z_0\rho_0 \; z_1\rho_1 \; \rho\mathbf{u} \; Ez)^T$, Res_c is the residual, and α is the ratio between time step Δt and the area of cell c.

Besides, the edges are separated stored into two lists [10]: LeafEdgeList for leaf edges and MotherEdgeList for non-leaf edges (Fig. 1(b)). Thus, the residual could be calculated in an edge-based manner. That is, the residual ($\mathrm{Res}_{f1\to L}$) at the left neighboring cell center ($f1 \to L$ or cell C in Fig. 2) of a leaf edge $f1$ is updated in the following way,

$$\mathrm{Res}_{f1\to L} = \mathrm{Res}_{f1\to L} + \Phi_{f1}\big(U^-, U^+, \mathbf{n}_{f1}\big)\cdot \Delta l_{f1}, \tag{28}$$

and the residual ($\mathrm{Res}_{f1\to R}$) at the right cell center ($f1 \to R$ or cell E in Fig. 2) of this leaf edge $f1$ is updated by

$$\mathrm{Res}_{f1\to R} = \mathrm{Res}_{f1\to R} - \Phi_{f1}\big(U^-, U^+, \mathbf{n}_{f1}\big)\cdot \Delta l_{f1}, \tag{29}$$

where Δl_{f1} denotes the length of the edge $f1$.

The numerical flux Φ_f in Eq. (28) and Eq. (29) is calculated by the Harten, Lax and van Leer approximate Riemann solver with the Contact wave restored (HLLC) scheme,

$$\Phi_f\big(U^-, U^+, \mathbf{n}_f\big) = \frac{1}{2}\big[\phi^- + \phi^+ - \mathrm{sign}(k_m)\big(U^+ - U^-\big)\big], \tag{30}$$

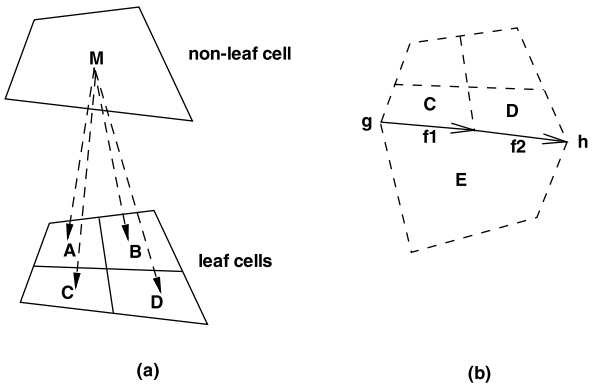

Fig. 2 Data structures for the cells and edges

with

$$\phi^j = F\left(U^j\right) \cdot \mathbf{n}_f + k_j^{\#}\left(U^{j*} - U^j\right), \quad j = -, +. \tag{31}$$

Here, $k_j^{\#}$ and U^{j*} are the intermediate velocity and states respectively, and k_m is the signal velocity [10].

It is clear that the calculation of the numerical flux only requires the left state and right state of the edge. These two states are calculated according to Hermit interpolation from the cell centers of both sides of the edge. So, in contrast to [3], there is no need to handle the handing nodes and no special treatment at the interface between the finer cell and the coarse cell.

In addition to the considering the convection numerical flux, the residual should be updated in the following way in order to solve Eq. (2),

$$\mathrm{Res}_{c,6} = \mathrm{Res}_{c,6} - z_c^n \sum_f (u_n)_f \cdot \Delta l_f, \tag{32}$$

where $(u_n)_f$ is the normal velocity at the edge and is computed in an HLLC consistent way [10].

Note that the numerical flux Φ_f is calculated once for each non-leaf edge which has no sub-edges before the updating of the residual (Eqs. (28), (29), and (32)). There is no need to calculate the numerical flux for a non-leaf edge. For example, the right neighboring cell of non-leaf edge $\overrightarrow{gh}$ is the same as the right neighboring cell of leaf edges $f1$ and $f2$, that is, $f1 \to R = f2 \to R = \overrightarrow{gh} \to R = E$. Thus, the residual at the right leaf cell center of this non-leaf edge $\overrightarrow{gh}$ is automatically updated by the operations (Eq. (28) and Eq. (29)) of its two sub-edges $f1$ and $f2$. This reduces the calculation of the numerical flux for the non-leaf edges as well as keeps the conservation of the numerical flux.

4 Results

To demonstrate the ability of the present adaptive solver for compressible multi-fluid flows with two different types of EOS, two cases with three different types of

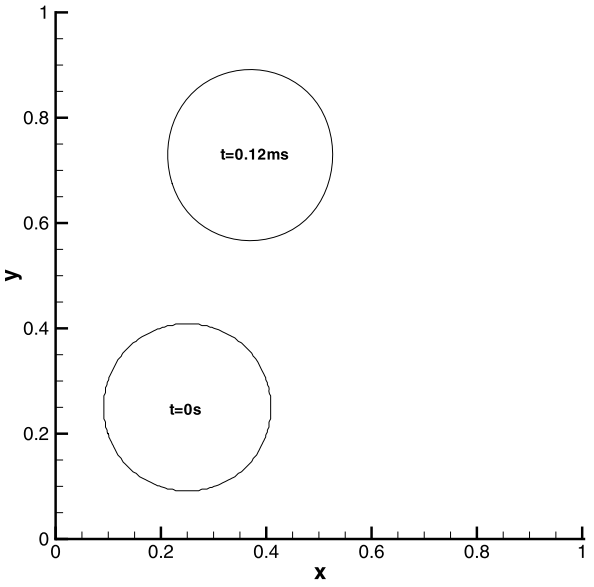

Fig. 3 Comparison of interface shape at $t = 0$ s and $t = 0.12$ ms

EOS, i.e., the van der Waals EOS, the stiffened gas EOS, and the Tait's EOS are used.

4.1 Interface Translation Problem

The interface translation problem is used to demonstrate the oscillation-free feature of current solver for compressible two-fluid flows with two different types of EOS. Note that there is no other fluid-mixture model which has shown the feature. To set up the problem, one fluid with a circular shape surrounded by another fluid is put at the center position of the domain. The surrounded fluid is modeled by the van der Waals EOS (Eq. (9) with the parameters $\gamma_1 = 1.4$, $a_1 = 5$, $b_1 = 1 \cdot 10^{-3}$). The inner fluid is modeled by the Tait's EOS ($\Gamma_i(\rho_i) = \gamma_i$, $\Pi_i(\rho_i) = \gamma_i(b_i - a_i)$) with the parameters as $\gamma_0 = 7.0$, $a_0 = 0$, $b_0 = 3.0 \cdot 10^8$. The radius of the circular interface is ($r_0 = 0.16$ m). The velocity and pressure are uniform ($\mathbf{u} = (1.0 \cdot 10^3$ m/s, $4.0 \cdot 10^3$ m/s), $P = 1.0 \cdot 10^5$ Pa) in the whole field. The initial densities are 1000 kg/m^3 for the inner fluid and 50 kg/m^3 for the surrounded fluid.

Since there are no shock and other perturbation in the flow field, it is expected that the inner fluid with circular shape should move with the constant velocity. The interface positions at $t = 0$ s and $t = 0.12$ ms are plotted in Fig. 3. It can be easily observed that the shape of the interface at $t = 0.12$ ms is almost the same as the initial one. Figures 4 and 5 display the pressure and velocity profiles. It is clear that there are no oscillations around the interface. All these show that the current solver can capture the interface accurately and preserve the oscillation-free property even though the fluids move across the mesh with different mesh spacing.

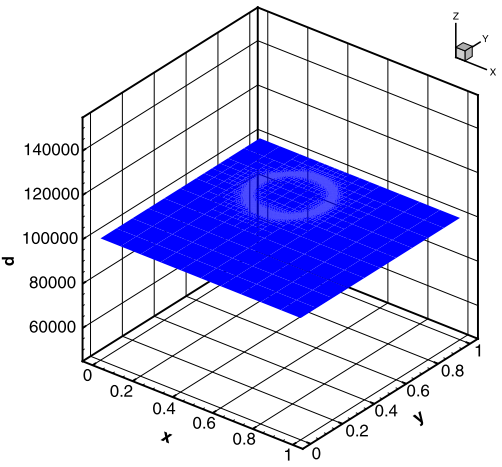

Fig. 4 Surface pressure profile at $t = 0.12$ ms

4.2 Bubble-Shock Interaction

In this section, an bubble shock interaction with two different types of EOS is considered [2, 5, 8]. Initially, a bubble gas with the radius 0.2 m is located at the (0.7 m, 0.5 m) of a water box with the domain $[0, 1.2] \times [0, 1]$ m^2. Here, the air is modeled by the van der Waals EOS and the water is modeled by the stiffened gas EOS ($\Gamma_i(\rho_i) = \gamma_i$, $\Pi_i(\rho_i) = \gamma_i a_i$) with the parameters as $\gamma_1 = 4.4$ and $a_1 = 6.0 \cdot 10^8$. A left going planar shock wave with Mach number of 1.422 is located at 0.95 m and travels in the water. The air (with density 1.2 kg/m^3) and the water (with density 1000 kg/m^3) at the left of the shock position are at rest $\mathbf{u} = (0\ \text{m/s}, 0\ \text{m/s})$ and atmosphere condition ($P = 1.0 \cdot 10^5$ Pa). Thus, the density

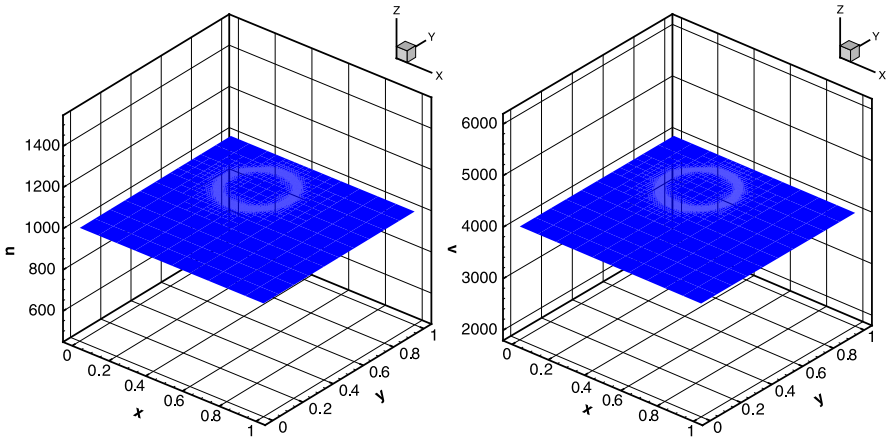

(a) U profile (b) V profile

Fig. 5 Surface velocity profiles at $t = 0.12$ ms

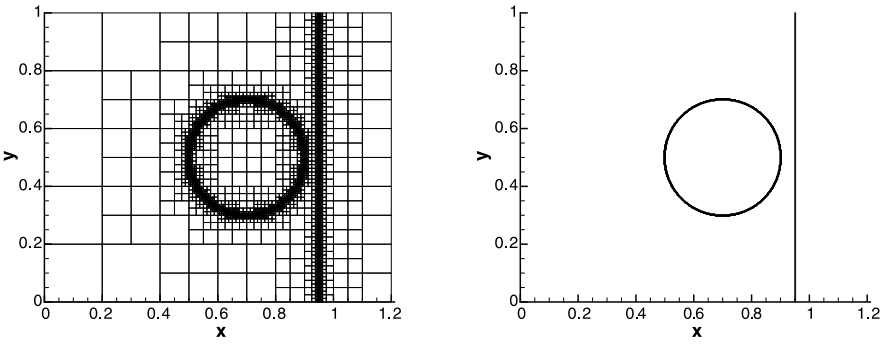

(a) Mesh (b) Density contour

Fig. 6 Mesh and density contour $t = 0$ s

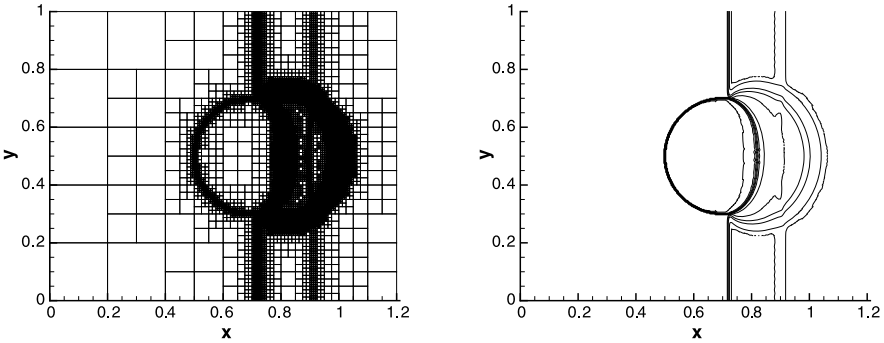

(a) Mesh (b) Density contour

Fig. 7 Mesh and density contour $t = 0.1$ ms

ratio (about 1000) and acoustic impedances (the density times the sound speed) ratio (about 3965) are very high [5].

The simulation is performed on the adaptive mesh generated by a uniform background mesh (level is 0) of 6×5 with the finest resolution level of 6. The reflective boundary conditions are employed at the top and bottom boundary, while the extrapolation boundary conditions are imposed at the left and right boundary. The results of mesh and density contour at different time (0 s, 0.1 ms, 0.2 ms, and 0.4 ms) are plotted in Figs. 6–9. It can be easily observed that the adaptive mesh can reflect the main flow features such as shock wave, rarefaction and material interface etc.

It also shows that it is suitable for unsteady flows. As can be seen in Fig. 6, the shock wave first propagates in the water. After the incident shock wave hits the bubble, a pair of refraction waves are generated and reflected from the interface (Fig. 7). As the shock wave propagates from the larger acoustic impedance medium of water into the lower acoustic impedance medium of air, these refraction waves are rarefaction waves. Besides, the shock wave also passes through the bubble and forms the

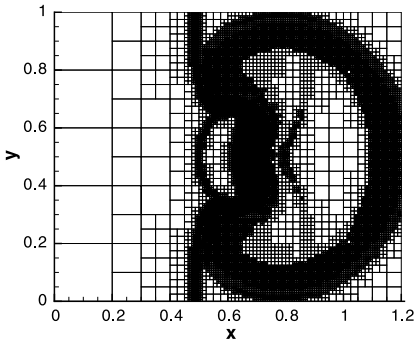

(a) Mesh

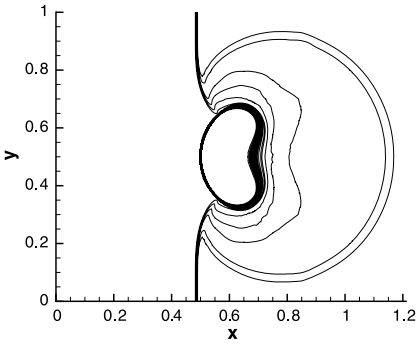

(b) Density contour

Fig. 8 Mesh and density contour $t = 0.2$ ms

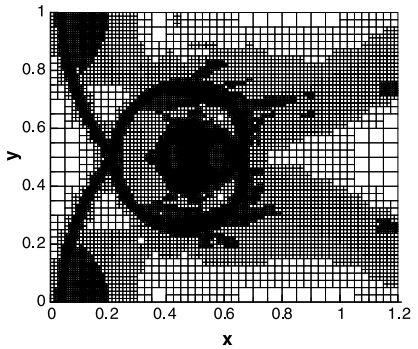

(a) Mesh

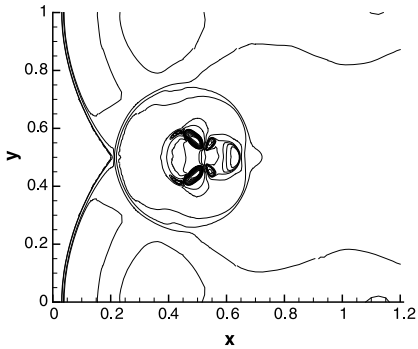

(b) Density contour

Fig. 9 Mesh and density contour at $t = 0.4$ ms

transmitted shock wave inside the bubble which is clearly captured by the adaptive mesh (Fig. 7(a)). With the increasing of the angle of incident shock wave and the interface, these refraction waves becomes the bifurcated Prandtl-Meyer wave. It attenuates the incident shock wave and results in the curved incident shock near the interface (Fig. 7(b)). Then the left-going shock wave continues to propagate through the bubble and the reflected circular wave moves outward. When the right moving circular wave hits the upper and lower boundary, the second reflected wave is generated (Fig. 8). The second reflected wave will interact with other waves to form a complex flow. Two small vortices are found to attach the bubble as shown in Fig. 9. The density and pressure profiles are plotted in Figs. 10, 11, 12, 13. It is clear that our results agree well with those of Shyue [5] which are obtained from the curves of [5] by using the software of Marisoft Digitizer.

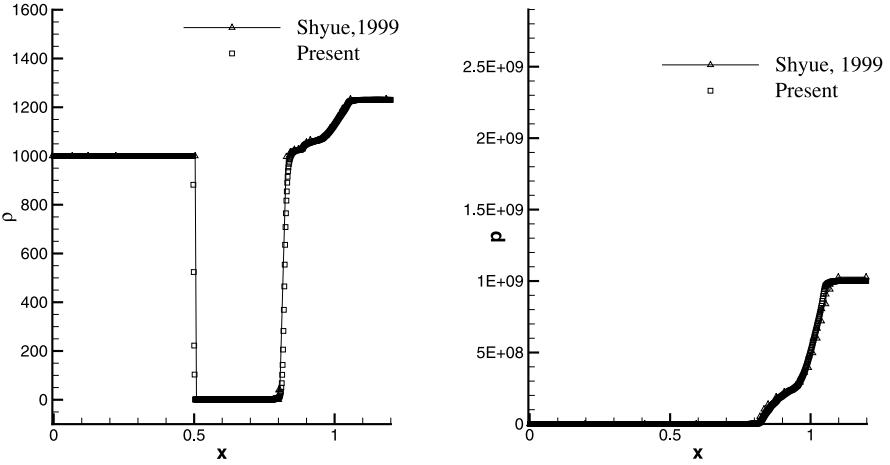

(a) Density profile (b) Pressure profile

Fig. 10 Comparisons of profiles at $t = 0.1$ ms

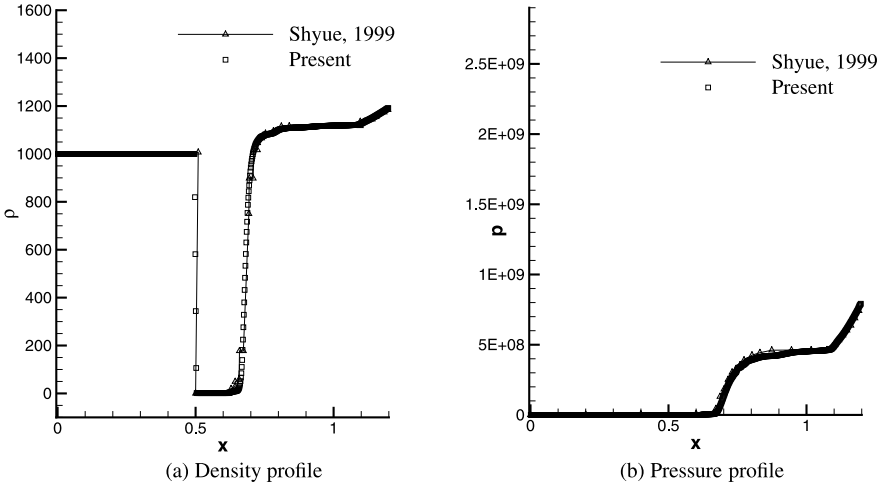

(a) Density profile (b) Pressure profile

Fig. 11 Comparisons of profiles at $t = 0.2$ ms

5 Conclusions

To tackle the challenging problems in compressible multi-fluid flows, an oscillation-free solution adaptive solver is proposed in this paper. It not only adaptively and accurately solves the problems with different types of EOS but also preserves the oscillation-free of velocity and pressure across the interface. Two test examples have been carried out to examine the performance of the present adaptive solver for multi-fluid flows with different types of EOS. The three commonly used equations of state

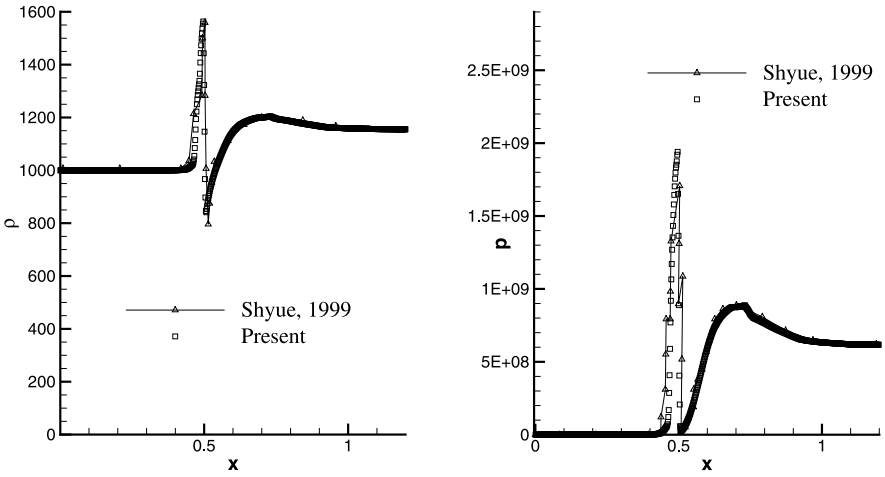

(a) Density profile (b) Pressure profile

Fig. 12 Comparisons of profiles at $t = 0.3$ ms

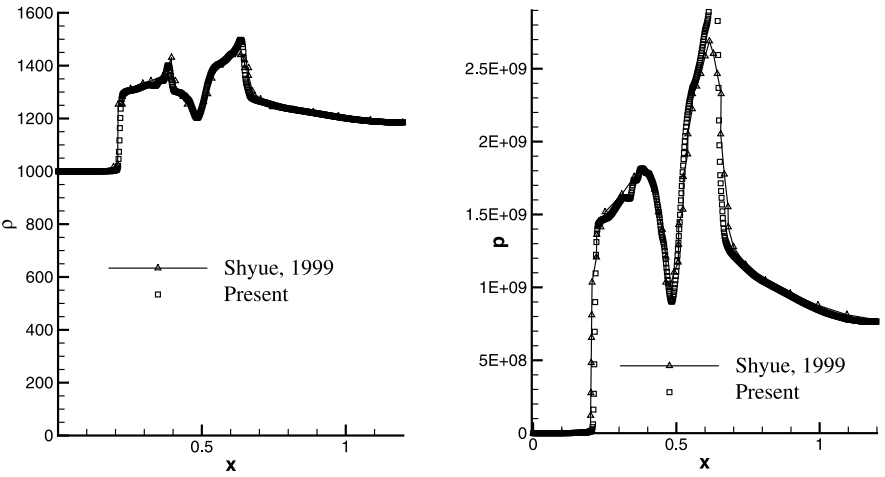

(a) Density profile (b) Pressure profile

Fig. 13 Comparisons of profiles at $t = 0.4$ ms

are involved in the calculations, namely, the van der Waals EOS, the stiffened gas EOS, and the Tait's EOS. Note that there is no other fluid-mixture model which has shown the oscillation-free feature for the problems with different types of EOS. Besides, the result of bubble shock interaction problem show that it could also be applied to problems with large density and acoustic impedances ratios.

References

1. Saurel, R., Massoni, J.: On Riemann problem based methods for detonation in solid energetic materials. Int. J. Numer. Methods Fluids **26**, 101–121 (1998)
2. Liu, T.G., Khoo, B.C., Yeo, K.S.: The simulation of compressible multi-medium flow. Part II: Applications to 2D underwater shock refraction. Comput. Fluids **30**, 315–337 (2001)
3. Nourgaliev, R.R., Dinh, T.N., Theofanous, T.G.: Adaptive characteristics-based matching for compressible multifluid dynamics. J. Comput. Phys. **213**, 500–529 (2006)
4. Kadioglu, S.Y., Sussman, M.: Adaptive solution techniques for simulating underwater explosions and implosions. J. Comput. Phys. **227**, 2083–2104 (2008)
5. Shyue, K.M.: A fluid-mixture type algorithm for compressible multicomponent flow with van der Waals equation of state. J. Comput. Phys. **156**, 43–88 (1999)
6. Shyue, K.M.: A fluid-mixture type algorithm for compressible multicomponent flow with Mie-Gruneisen equation of state. J. Comput. Phys. **171**, 678–707 (2001)
7. Saurel, R., Abgrall, R.: A multiphase Godunov method for compressible multifluid and multiphase flows. J. Comput. Phys. **150**, 425–467 (1999)
8. Allaire, G., Clerc, S., Kokh, S.: A five-equation model for the simulation of interfaces between compressible fluids. J. Comput. Phys. **181**, 577–616 (2002)
9. Banks, J.W., Schwendeman, D.W., Kapila, A.K., Henshaw, W.D.: A high-resolution Godunov method for compressible multi-material flow on overlapping grids. J. Comput. Phys. **223**, 262–297 (2007)
10. Zheng, H.W., Shu, C., Chew, Y.T.: An object-oriented and quadrilateral-mesh based solution adaptive algorithm for compressible multi-fluid flows. J. Comput. Phys. **227**, 6895–6921 (2008)
11. Larouturou, B.: How to preserve the mass fraction positive when computing compressible multi-component flows. J. Comput. Phys. **95**, 59–84 (1991)
12. Abgrall, R., Karni, S.: Computations of compressible multifluids. J. Comput. Phys. **169**, 594–623 (2001)
13. Shyue, K.M.: An efficient shock-capturing algorithm for compressible multi-component problems. J. Comput. Phys. **142**, 208–242 (1998)
14. Shyue, K.M.: A fluid-mixture type algorithm for barotropic two-fluid flow problems. J. Comput. Phys. **200**, 718–748 (2004)
15. Johnsen, E., Colonius, T.: Implementation of WENO schemes for compressible multicomponent flow problems. J. Comput. Phys. **219**, 715–732 (2006)